

RESEARCH ARTICLE

Open Access



Simultaneous removals of cadmium(II) ions and reactive yellow 4 dye from aqueous solution by bone meal-derived apatite: kinetics, equilibrium and thermodynamic evaluations

Edwin A. Ofudje^{1,2*} , Idowu A. Adeogun², Mopelola A. Idowu², Sarafadeen O. Kareem³ and Nelly A. Ndukwe¹

Abstract

The simultaneous removal of Cadmium ions and reactive yellow 4 dye (RY4 dye) by bone meal-derived apatite (BMDA) were investigated in a batch process. The structural elucidation of the prepared BMDA was done using TEM, XRD, FT-IR and EDX to evaluate the structures of the adsorbent. Different experimental features such as the agitation time, BMDA dosage, temperature, initial adsorbate concentration and pH of the solution were examined on the uptake pattern of the pollutants. The mechanism of adsorption was examined with Elovich, pseudo-first-order, intraparticle diffusion and pseudo-second-order kinetic models, while Langmuir, Dubinin-Radushkevich (D-R), Freundlich and Tempkin isotherms were exploited in order to describe the behaviour of the equilibrium process. Analysis from XRD revealed peaks corresponding to single phase apatite powder, while the various forces responsible for the interactions between the BMDA surface and the pollutants were obtained to CO_3^{2-} , OH^- and PO_4^{3-} as observed by FT-IR analysis. SEM and TEM investigations confirmed a round-like morphology which agglomerated together upon the adsorption of pollutants.

The kinetic modelling of the adsorption data were well illustrated with the pseudo-first-order model with correlation coefficient (R^2) values ranging from 0.997 to 0.999. Isotherms studies revealed that best fit was achieved with Langmuir isotherm with adsorption capacities of 94.85 and 116.16 mg/g for RY4 dye and Cd(II) ions respectively. Thermodynamic study signified the uptake of the pollutants to be spontaneous, feasible and endothermic in nature. The values of entropy change (ΔS) for the sorption processes calculated are 86.57 and 60.16 J/mol/K for Cd(II) and RY4 dye, respectively.

Keywords: Adsorption, Cadmium, Equilibrium, Apatite, Kinetics, RY4 dye

Introduction

Contamination of water body by heavy metals ions and dyes contained in discharged wastewater from various human and industrial activities had caused severe threats to the environment (Yang et al. 2012). Generated effluents from industrial activities

among which are mining, battery manufacturing, metallurgical and chemical industry often contain toxic heavy metal ions which cannot be degradable biologically and could amass in the tissue of living organisms, resulting into various health issues (Cheng et al. 2016; Zhao et al. 2011). Cadmium is a known toxic metal that can be readily available in some industrial workplaces, it is a major constituent of electronics components and also widely used in batteries, electroplating and in some industrial paints. It is a highly toxic and has been classified as the sixth most poisonous substance (Janeggitz et al.

* Correspondence: ofudjeandrew4real@yahoo.com; eaofudje@mtu.edu.ng

¹Department of Chemical Sciences, Mountain Top University, Prayer City, Ibafo, Nigeria

²Department of Chemistry, Federal University of Agriculture, Abeokuta, Nigeria

Full list of author information is available at the end of the article

2011). Cadmium even at low concentration may lead to bone degeneration, liver damage, kidney and respiratory tract problems and hypertension (Janeggitz et al. 2011).

The toxicity effects of water contaminations by dye pollutants are undesirable and can even be carcinogenic at very absurdly low concentrations (Shappur et al. 2017). Effluents from textile, food, plastics, paper and leather industries are laden with dye, which not only is toxic to aquatic life, but also can destroy the aesthetic nature of the water system by reducing photosynthesis activities and decreasing recreation activities of the stream (Allen et al. 2004; Shappur et al. 2017). Due to the fact that wastewater-containing dyes are stable to light, heat and oxidation, their treatments using the conventional methods, is a major challenge in the wastewater treatment. They display resistance to aerobic digestion and sometimes not biodegradable, and even when digested or degraded, hazardous and toxic by-products are produced due to the presence of aromatic ring structures in most of the dyes molecules (Shawabkeh and Tutunji, 2004; Sun and Yang, 2003).

Various conventional technologies have been developed for remediation of contaminated wastewater and they are filtration, ion exchange, adsorption, electrodeposition, chemical precipitation and membrane systems (Barakat, 2011; Ngah et al. 2011; Schmuhl et al. 2001; Shukla and Pai, 2005; Wang et al. 2005). Although many of these technologies have various advantages, their applications had been limited by the high cost of operations, generation of secondary waste and ineffective complete removal of contaminants (Adeogun et al. 2013; Rengaraj et al. 2004; Shukla and Pai, 2005; Wang et al. 2005; Xiao-qin et al. 2017). Comparatively, adsorption had been adjudged the best technology in the treatment of wastewater owing to its easy handling and it does not produce toxic substances as by-products and is effective for the removal of different types of pollutants. In the wastewater treatment process, activated carbon has been used in a good number of times as an adsorbent due to its large specific surface area; however, its application is reduced owing to its high cost of production (Shappur et al. 2017). Hence, continued research towards alternative adsorbents (which are inexpensive with excellent sorption efficiencies) is justified.

The potentials of several varieties of adsorbents for the elimination of different pollutants have been explored in the remediation of wastewater with good results (Ngah et al. 2011; Shukla and Pai, 2005; Wang et al. 2005). Calcined bone contains apatite which is a stable form of the calcium phosphates

with good biocompatibility and widely used in biomedical applications (Nasser et al. 2009). Apatite has been utilized for the uptake of contaminants in soil and purification of waste waters (Chen et al. 1997; Feng et al. 2010; Nzihou and Sharrock, 2010; Smiciklas et al. 2006).

In this study, a cheap adsorbent from calcined animal bones was prepared and then characterized with the use of XRD, SEM, energy-dispersive X-ray (EDX), FT-IR and TEM. The prepared adsorbent was thereafter used in a batch process for simultaneous uptake of Cd(II) ions and reactive yellow 4 dye (RY4 dye) from aqueous solutions. The roles of different experimental conditions such as initial contaminants concentration, contact time, pH and adsorbent dosage were looked into. Also, the kinetics, equilibrium and thermodynamics of the adsorption process were evaluated.

Experimental

Synthesis of adsorbent

Waste animal bones were collected from an Abattoir at Abeokuta, Nigeria. Collected bone samples were steam washed to remove sand, fat, marrow and attached flesh. The raw materials were treated with 0.1 M solution of NaOH, washed with distilled water and thereafter dried in an oven at a temperature of 110 °C overnight and milled into smaller pieces and calcined at a temperature of 1000 °C using a heating rate of 5 °C/min in air box furnace. The residue was ground into fine powder, sieved and designated as bone meal-derived apatite (BMDA) and stored in an airtight container before use. The schematic representation for the synthesis of the adsorbent and its subsequent use for the adsorption of pollutants is represented in Fig. 1.

Characterizations

The evaluation of the chemical composition of BMDA was done using a scanning electron microscope (Hitachi, Japan, S-3000H) with EDX incorporated. Information about the phase purity and crystallinity was done using X-ray diffractometer (PANalytical, X'Pert PRO, Netherland) in a step size of 0.02 using CuK α ($\gamma = 1.54178 \text{ \AA}$) radiation over the range of 10 to 60°. Fourier-transform infrared (FT-IR) spectroscopic analysis was performed between 400 and 4000 cm^{-1} with the aid of TENSOR 27 spectrometer (Bruker, Germany) and by adopting the KBr pellet method. Transmission electron microscope (TEM) analysis was done on (TEM; Tecnai 20 G2 FEI, the Netherland). A Zetasizer Nano ZS instrument (Malvern, UK) was used to evaluate the value of the zeta potential of the fish scale-derived hydroxylapatite powder. 0.1 g of the apatite

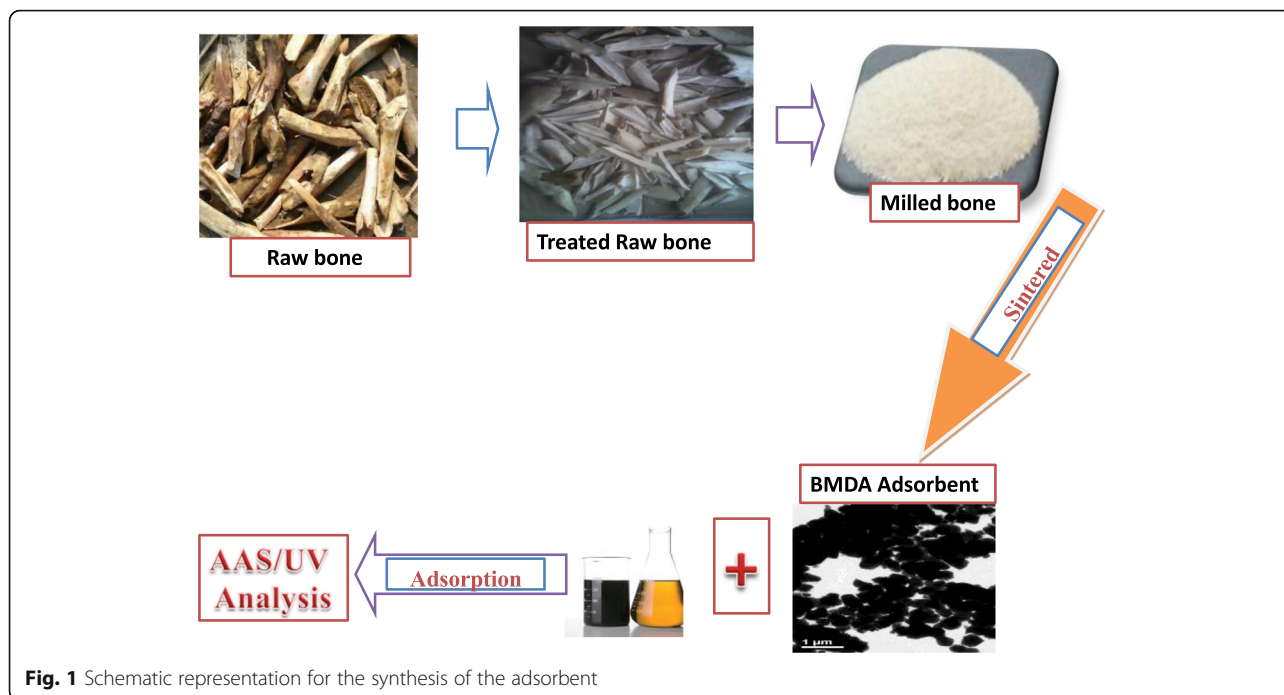
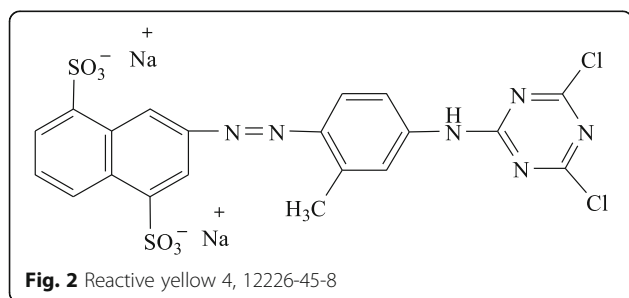


Fig. 1 Schematic representation for the synthesis of the adsorbent

powder was dissolved in 25 mL of pollutant solution, while pH adjustment was achieved with 0.1 M HCl and NaOH solution. The thermal stability of the prepared BMDA was performed with the aid of Thermogravimetric analysis (TGA) using SDT Q600 V8.3 Build 101simultaneous DSC-TGA instrument.

Preparations of aqueous solution of Cd(II) ions and RY4 dye

A stock solution containing Cd(II) and reactive yellow 4 dye were prepared from Cd (NO₃)₂ · 4H₂O (99%) (Aldrich, Germany) and reactive yellow 4 dye (BDH, London), the structural formula of which is shown in Fig. 2. Solutes were accurately weighed such that the solution contained 1 g equivalent each of the metal ion and dye in 1 L de-ionised water, working solutions of the pollutants were then made using the stock by dilution method. Before the addition of the adsorbent, pH adjustment to a desired value was achieved with the addition of HCl or NaOH (1.0 mol L⁻¹).



Equilibrium studies

The batch equilibrium experiment was done in 250-ml Erlenmeyer flasks which contain 100 ml solution of initial concentrations of Cd(II) ions and RY4 dye ranging from 40 to 240 mg/L with BMDA of 1.4 g/L. A thermostat shaker set at 150 rpm and 30 ± 1 °C was utilized to equilibrate the contents for 120 min. The Cd(II) and RY4 dye concentrations in the solutions at initial stage and after the adsorption process were evaluated using Atomic Absorption Spectrophotometer (Varian Model SPECTRA 220) and UV-vis spectrophotometer (UV-VIS-NIR VARIAN 500 Scan CARY), respectively. The differences between initial concentration added to the adsorbent and that of the supernatant concentration was estimated using:

$$Q_e = \frac{C_o - C_e}{m} \times V \quad (1)$$

where the amount of adsorbate adsorbed (mg/g), the initial and equilibrium concentrations (mg/L) are given as Q_e , C_o and C_e respectively, V stands for volume (L) of the pollutant taken and the adsorbent mass (g) is denoted as m .

Kinetics studies

In the evaluation of the kinetics study, samples were collected at preset time intervals (0, 5, 10, 15, 30, 60, 120, and 240) and analysed for the metal ions and RY4 dye contents. The contents of the contaminants sorbed at a

particular time t , which is represented as Q_t (mg g^{-1}), was estimated using the expression below:

$$Q_t = \frac{(C_o - C_t)V}{W} \quad (2)$$

given that the concentrations of the metal ions and dye at time t is C_t (mg L^{-1}), respectively, C_o (mg L^{-1}) and V (L) are as previously defined, while W is the mass (g) of dry adsorbent used.

Adsorption isotherms

Freundlich, Dubinin-Radushkevich, Langmuir and Tempkin isotherms were used for the analysis of the equilibrium studies. Micro Math Scientist software was used to evaluate the correlation coefficients, R^2 which was estimated from the least square fit statistic and was used to determine the suitability and acceptability of the isotherms.

Langmuir isotherm

Langmuir isotherm is given by Eq. 3 based on assumptions that interactions do not exist between molecules adsorbed and that the whole surface for the adsorption process has the same sorption activity (Adeogun and Babu, 2015; Langmuir, 1918):

$$Q_{eq} = \frac{Q_{max}bC_e}{1 + bC_e} \quad (3)$$

where Q_{max} and C_e (mg g^{-1}) stand for the maximum amount of solute sorbed and the adsorbate concentration remaining in the solution at equilibrium and the equilibrium constant is given as b ($\text{dm}^3 \text{mg}^{-1}$). The separation factor (R_L) was described in the relationship below (Adeogun et al. 2018):

$$R_L = \frac{1}{1 + bC_o} \quad (4)$$

b stands for the Langmuir equilibrium constant (L mg^{-1}) and C_o has been previously defined. The R_L value of $0 < R_L < 1$ indicates favourable adsorption process, and linear when $R_L = 1$, unfavourable when $R_L > 1$, and when $R_L = 0$, it is irreversible.

Freundlich isotherm

Freundlich isotherm which is used to explain adsorption taking place on a heterogeneous surface and can be presented as (Adeogun et al. 2013; Chen et al. 1997; Nzihou and Sharrock, 2010; Smiciklas et al., 2006):

$$Q_{eq} = K_F C_e^{1/n} \quad (5)$$

given that the adsorption capacity and the adsorbent intensity are represented as K_F and n , respectively.

Tempkin adsorption isotherm

Tempkin isotherm assumed that the surface coverage determined the free energy of adsorption and it takes into considerations, the interface between sorbent and adsorbate (Adeogun et al. 2018; Chen et al. 1997; Shappur et al. 2017). The model is as presented in Eq. 6:

$$Q_e = \frac{RT}{b_T} \ln a_T C_e \quad (6)$$

where a_T and b_T are the Tempkin constants relating to binding constant (Lmg^{-1}) at equilibrium and the heat of adsorption, respectively, T is the temperature (K) and the ideal molar gas constant ($8.314 \text{ J mol}^{-1} \text{ K}^{-1}$) is given as R .

Dubinin-Radushkevich isotherm

The D-R equation which is normally used in explaining the adsorption behaviour which occurs in microporous materials and is based on the supposition that alteration in the potential energy between the sorbed molecules and gas substance and also the surface homogeneity on microscopic behaviour (Adeogun and Babu, 2015). It is more general when compared with that of the Langmuir isotherm and can be used to classify adsorption processes into physisorption or chemisorption and can be equally used to determine the surface energy heterogeneity and is given as:

$$Q_e = Q_s e^{-\beta \epsilon^2} \quad (7)$$

where Q_s represents the saturation capacity (mol g^{-1}), the Polanyi potential (ϵ) is given by the relation, $\epsilon = \ln(1 + \frac{1}{C_e})$, where R ($\text{J mol}^{-1} \text{ K}^{-1}$), C_e (mg L^{-1}) and T (K) are as previously described. The values of the constant β ($\text{mol}^2 \text{ J}^{-2}$) can be used to determine the mean free energy E (kJ mol^{-1}) of the adsorption process per molecule of the pollutants as the solid is transferred from the solution onto the surface of the adsorbent (Adeogun and Babu, 2015; Adeogun et al. 2018). The expression in Eq. 8 relates β to the mean free energy of adsorption of the adsorbate.

$$E = (2\beta)^{-0.5} \quad (8)$$

The process of adsorption is described as chemisorption if the values of E are between 8 and 16 kJ mol^{-1} , but if the magnitudes of E are less than 8 kJ mol^{-1} , it suggests a physisorption process.

Adsorption kinetics studies

In order to examine the mechanisms of the adsorption process, pseudo-first-order and pseudo-second-order, intraparticle diffusion and Elovich kinetic models were

utilized to explain the data obtained from the time-dependent adsorption studies of Cd(II) and RY4 by BMDA. The least square fit was also used to obtain various the parameters.

The pseudo-first-order kinetics model

The pseudo-first-order kinetic model is represented in Eq. 9 below (Lin and Brusick, 1992):

$$\frac{dQ}{dt} = k_1(Q_e - Q_t) \quad (9)$$

where Q_e and Q_t are as previously defined, respectively; k_1 stands for the adsorption rate constant (min^{-1}); and t represents the contact time (min). Upon integration and rearrangement, within the limit of $Q_t = 0$ at $t = 0$, and $Q_t = Q_t$ at $t = t$, eq. 9 can be transformed to:

$$Q_t = Q_e(1 - e^{-k_1 t}) \quad (10)$$

The least square fit of Q_t versus t at various solutes concentrations was used to estimate the parameters Q_e and k_1 of the model (Adeogun and Babu, 2015).

The pseudo-second-order kinetics model

The pseudo-second-order kinetics model can be described using Eq. 11 below (Adeogun et al. 2012):

$$t / Q_t = 1 / k_2 Q_e^2 + \left(1 / Q_t\right) t \quad (11)$$

The expression above can also be rearranged to give Eq. 12 below:

$$Q_t = \frac{k_2 Q_e^2 t}{1 + k_2 Q_e t} \quad (12)$$

where rate constant of pseudo-second-order process is given as k_2 ($\text{g mg}^{-1} \text{min}^{-1}$). The physical parameter values were obtained using the least square fit of Q_t versus t at various solutes concentrations.

Elovich model

The Elovich kinetic model proposed that the rate of adsorption of adsorbate onto the adsorbent surface decreases exponentially with an increase in the adsorbed molecules (Shappur et al., 2017). It is a kinetic model dedicated to chemisorption process and generally expressed as shown in Eq. 13 (Shappur et al. 2017):

$$Q_t = 1 / \beta \ln(\alpha \beta * t) \quad (13)$$

where α ($\text{mg g}^{-1} \text{min}^{-1}$) denotes the initial adsorption rate and the desorption constant is given by β (g mg^{-1}). The reciprocal of β shows the quantity of available empty adsorption sites of pollutants and the expression

$1 / \beta \ln(\alpha \beta)$ gives the value of adsorbed molecules when t is equal to zero.

Intraparticle diffusion model

Information from the kinetic models alone cannot provide sufficient explanation about the diffusion mechanism of the sorption process; hence, the application of the intraparticle diffusion model (eq. 14). The model shows that the initial diffusion rate is a function of time and surface resistance created by the concentration gradient across the surface (Adeogun and Babu, 2015; Ofudje et al. 2017).

$$Q_t = K_{id} t^{0.5} + C_i \quad (14)$$

where K_{id} ($\text{mg g}^{-1} \text{min}^{-0.5}$) and C_i stand for the intraparticle diffusion rate constant and the measurement of the surface thickness of the adsorbent, respectively.

Thermodynamics of adsorption process

The distribution of the solutes particles between the adsorbent and solution at equilibrium is written as (Adeogun et al. 2012; Ofudje et al. 2017):

The equilibrium constant, K_d can be expressed according to the concentrations in each of the media:

$$K_d = \frac{\text{Solute}_{\text{adsorbed}}}{\text{Solute}_{\text{solution}}} \quad (15)$$

$$K_d = \frac{Q_e}{C_e} \quad (16)$$

The equilibrium constant K_d can be used to determine the thermodynamic such as standards entropy change (ΔS°), enthalpy change (ΔH°) and free energy change (ΔG°) since it is a temperature-dependent constant using the following relation:

$$\Delta G^\circ = -RT \ln K_D \quad (17)$$

$$\Delta G^\circ = \Delta H^\circ - T \Delta S \quad (18)$$

$$\ln K_d = \Delta S^\circ / R - \Delta H^\circ / RT \quad (19)$$

The linear plots of $\ln K_d$ versus the inverse of temperature ($1/T$) which should produce a straight line with slope as ΔS° and intercept of ΔH° and respectively. Spontaneity, heat change and randomness at interphase during adsorption can be estimated from the values of ΔG° , ΔH° and ΔS° .

Statistical test

The need to compare error distribution becomes imperative since least square fit was use to evaluate the kinetic parameters. Generally, the acceptability or otherwise of the models are based on the values of the

correlation coefficients, R^2 . To this end, three error functions, namely the sum of square error function (SSE), root mean square error (RMSE) and composite fractional error (HYBRID), (Eqs. 20–22) were used to validate the fitness of kinetic models tested in this present studies (Shappur et al. 2017).

$$\text{SSE} = \sum_{i=1}^N \left(Q_{(\text{exp})} - Q_{(\text{cal})} \right)^2 \quad (20)$$

$$\text{RMSE} = \sqrt{\frac{\sum_{i=1}^N \left(Q_{(\text{exp})} - Q_{(\text{cal})} \right)^2}{N}} \quad (21)$$

$$\text{HYBRD} = \frac{100}{N-P} \sum_{i=1}^N \frac{\left(Q_{(\text{exp})} - Q_{(\text{cal})} \right)}{Q_{(\text{exp})}} \quad (22)$$

N denotes the data points, P stands for the numbers of the parameters in the model. The lower the values of SSE, RMSE and HYBRID errors and higher the value of R^2 , the more the suitability of the model.

Results and discussions

Characterization of BMDA

Surface morphological analyses of the BMDA by SEM and TEM before and after adsorption are presented in Fig. 3. The SEM results showed a round-

like morphology which agglomerated together after adsorption of pollutant as depicted in Fig. 3 a and b, respectively. This was equally confirmed by TEM analysis with an agglomerated round particle with length varying in the range of 20 to 60 nm and width of 3–9 nm as shown in Fig. 3 c and d. However, upon adsorption (Fig. 3d), the morphology appeared bigger when compared with Fig. 3 c. The SAED (as inserted in Fig. 3c & d) patterns showed that the polycrystalline structure was transformed into amorphous apatite after the incorporation of the solutes with the disappearance of a sharp spotted continuous ring suggesting an amorphous apatite which is in good agreement with the FT-IR and XRD results as shown in Figs. 4 and 7 below, respectively.

The FT-IR spectra of BMDA before and after pollutants adsorption are represented in Fig. 4, the fundamental vibration modes of PO_4 groups of the apatite structure are shown by the band at 560 and 1030–1100 cm^{-1} . Bands appearing at 865 and 1465 cm^{-1} were assigned to residual carbonate arising from the precursor's bone, while broad bands at 1650 and 3450 cm^{-1} were ascribed to H-O-H bands and OH signals, respectively. A shift in band position and broadening of peaks were prominent after the adsorption, suggesting a further interaction between the adsorbate and the synthesized apatite powder.

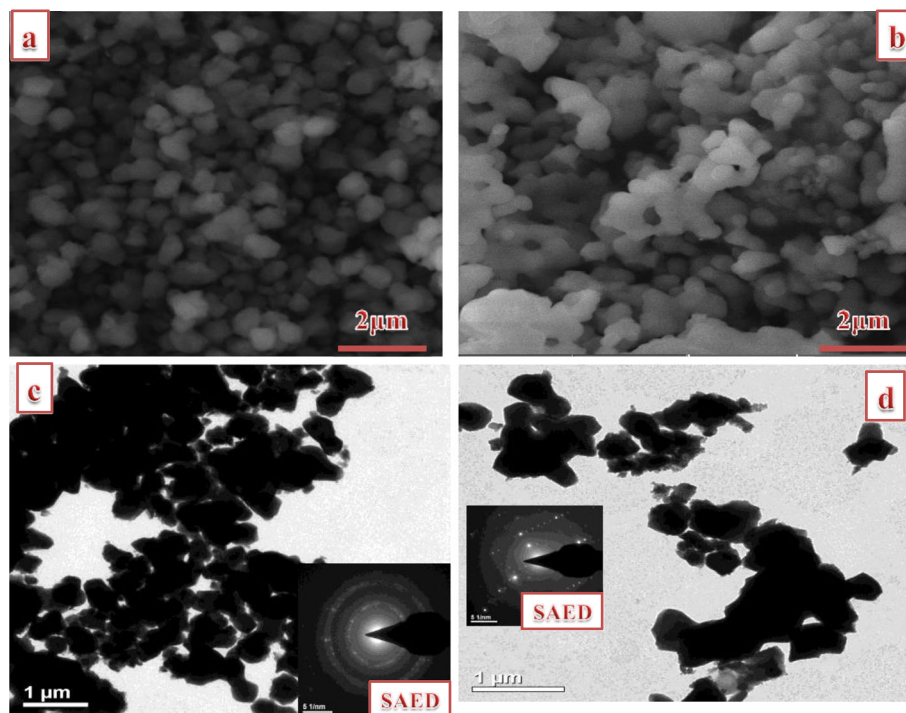


Fig. 3 SEM and TEM images of BMDA before sorption and after pollutants sorption

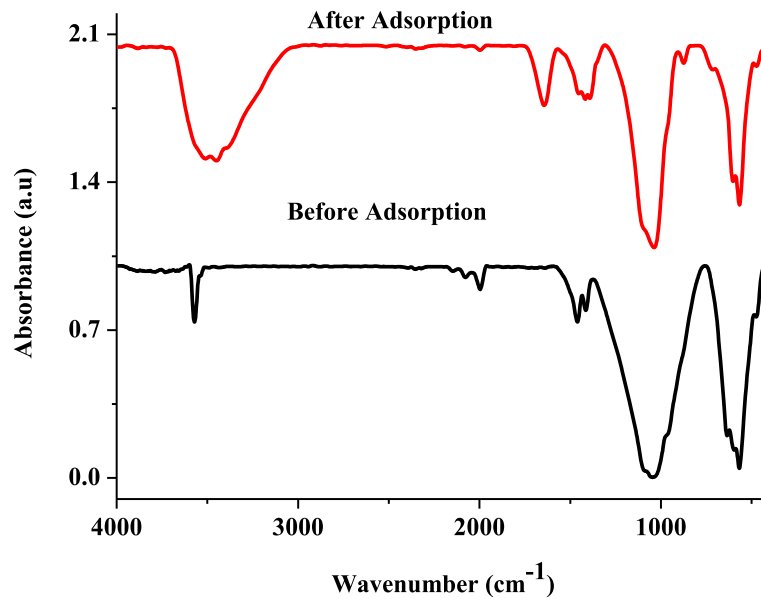


Fig. 4 FT-IR analysis of BMDA before adsorption and after adsorption

EDX analysis of the fabricated BMDA is as indicated in Fig. 5 suggesting the presence of Ca, P, C, O, Mg, Si, K and Na in the apatite lattice. The trace elements in the adsorbent could be traced to those inherent in the precursor (bone); hence, EDX result

suggested a non-stoichiometric apatite with Ca/P of 2.02. The loss of water, removal of organic portion and the decomposition of BMDA were evaluated with the aids of TGA and DTA analysis as presented in Fig. 6. The three successive behaviours indicating

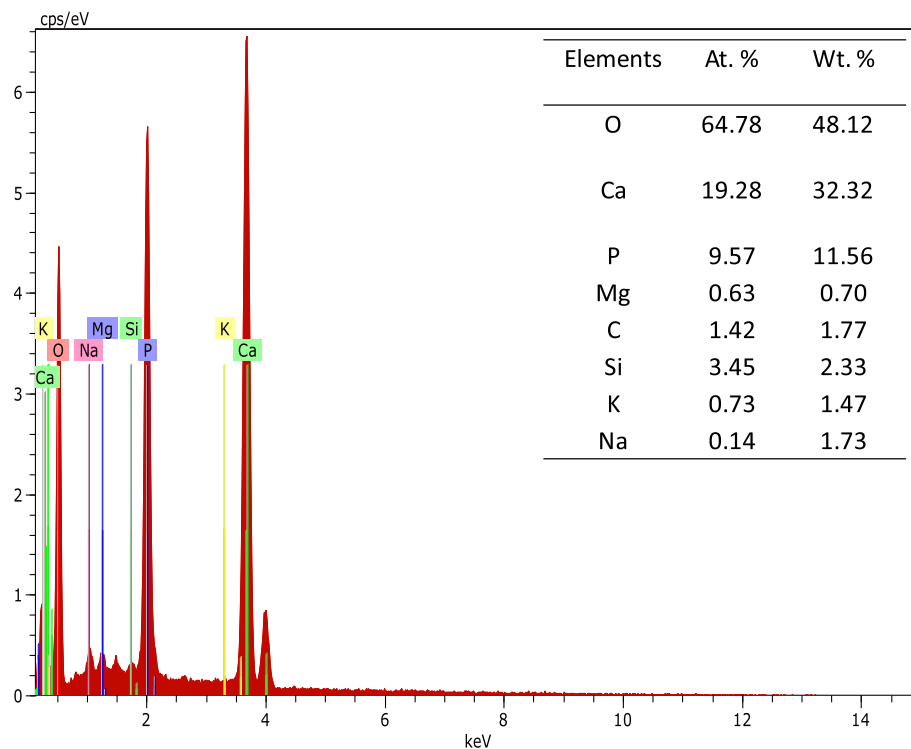
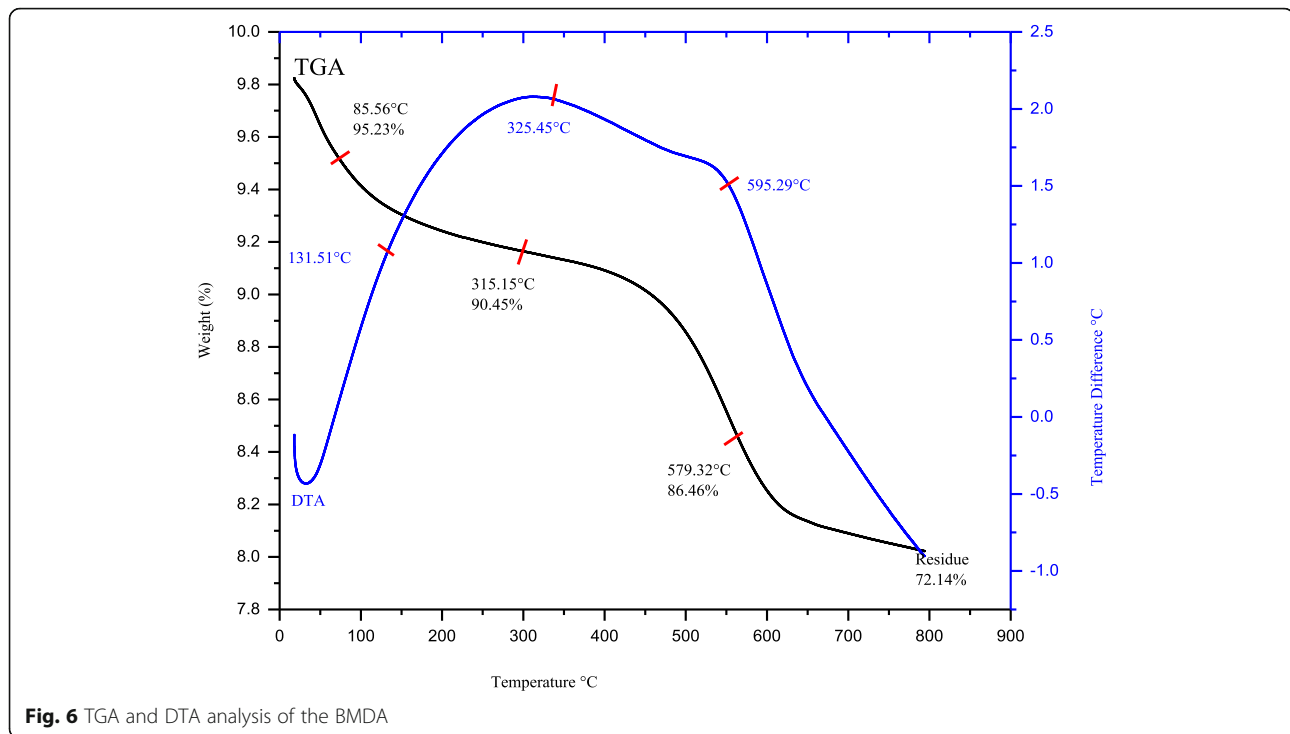
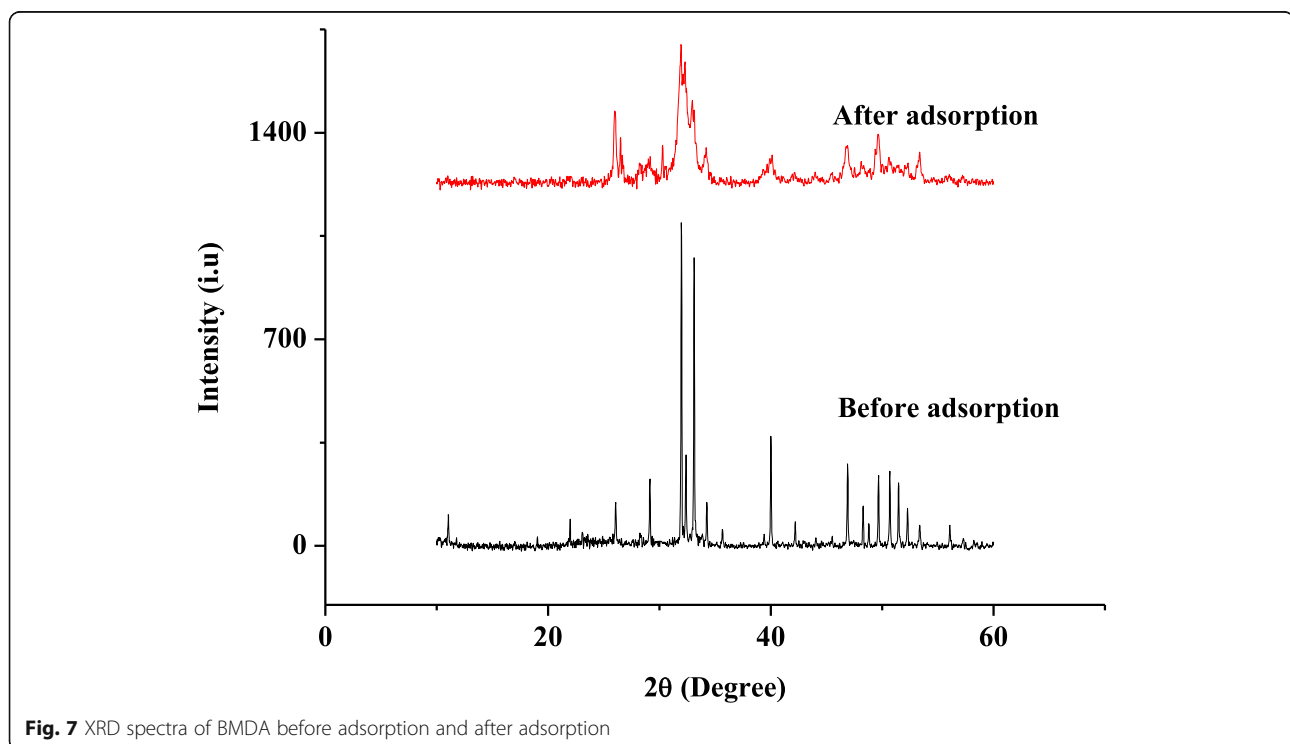


Fig. 5 EDX analysis of BMDA



weight loss in the raw material were observed. Weight loss of 4.77% was noticed at 85.56 °C and this could be ascribed to removal of surface water from the biomass and was confirmed by DTA with an endothermic loss at 131 °C. The weight loss of 9.55% noticed

at 315.15 °C could be attributed to the elimination of the organic contents from the biowaste with DTA exothermic confirmation at 325 °C. The final weight loss of 13.54% observed at 579.32 °C is as a result of the decomposition of carbonate with an exothermic



loss at 595 °C as confirmed by DTA, thus leaving a residual weight of 72.14% of the prepared adsorbent.

X-ray diffraction spectra of BMDA before and after pollutants adsorption are presented in Fig. 7. It was observed that peaks of synthesized powders correspond to characteristic peaks of pure HAp powder using the standard JCPDS (09-432). Well-resolved characteristic peaks of HAp powder were obtained at 2θ value of 25.99° and 31.87° corresponding to (002) and (211) planes, respectively, with the peak at the 2θ value of 31.87° having the highest intensity. The phase formed was pure as there were no traces of other phases. Other standard planes observed in the XRD analysis by the JCPDS card are (202), (210), (222), (213), (300), (322), (004, 410) corresponding to pure or single HAp powder. The synthesized powder showed highly polycrystalline phase with the appearance of many sharp peaks. However, with the incorporation of the adsorbate onto the apatite, although no new phase was observed; however, these sharp peaks became less, broad and with reducing intensity indicating an amorphous apatite. Amorphous substances do not possess long range of Bragg peaks in X-ray diffraction order. So the diffraction from them do not show sharp Bragg peaks as observed in the XRD spectrum of the apatite after the adsorption of the pollutant. The crystallite sizes of the adsorbent were estimated using the Debye-Scherrer equation (Fumiaki et al. 2005):

$$D_{(hkl)} = \frac{K\lambda}{\beta \cos\theta} \quad (23)$$

where D represents the crystallite size in nanometres, maximum of the peak at half of the maximum intensity, FWHM (in degree) is given as β , λ is the diffraction wavelength (0.154 nm) and θ is the diffraction angle; K stands for constant related to the crystallite shape and is approximately 0.94. The hexagonal crystal parameters were equally computed from the following equation:

$$\frac{1}{d_{(hkl)}} = \left\{ \frac{4(h^2 + k^2 + kh)}{3a^2} + \frac{i^2}{c^2} \right\}^{1/2} \quad (24)$$

where the distance between adjacent planes in the set of Miller indices ($h k l$) in nanometres is given as d and a , b and c represent the lattice parameters. The unit cell

volume (V) of the apatite was computed from the equation below:

$$V = 2.589(a^2).c \quad (25)$$

Table 1 shows the values of the lattice parameters and the crystallite size before and after adsorbate sorption. As indicated, the crystallite size increases after adsorption which is due to the incorporation of the respective adsorbate onto the apatite. Lattice parameter ' a ' increases after the incorporation of the adsorbate, while lattice parameter ' c ' and ' v ' decrease.

Effects of agitation time and initial pollutants concentrations on sorption capacities

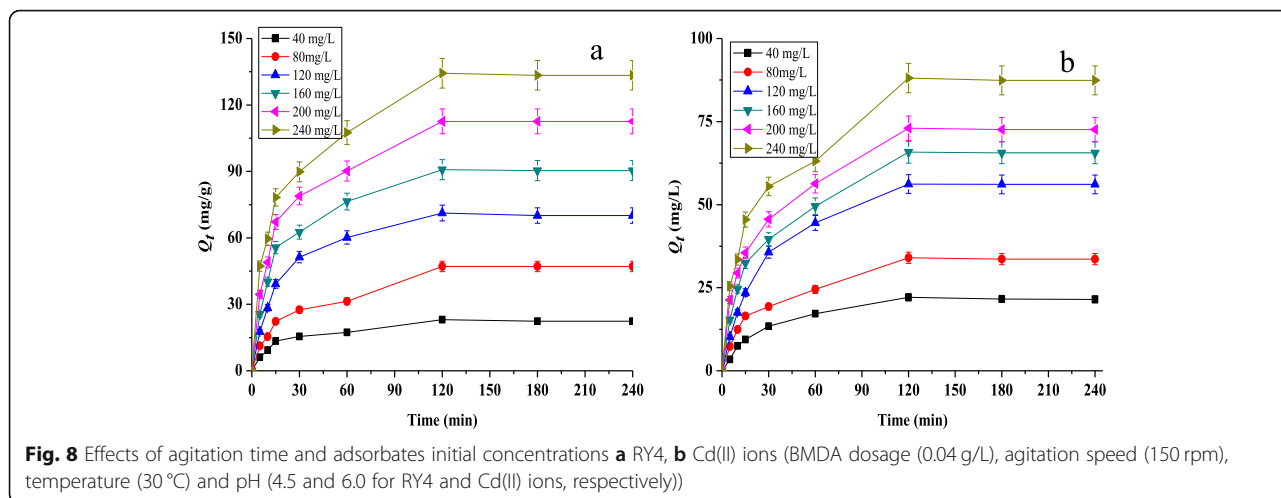
The roles of contact time and initial pollutants concentrations on the removal of Cd(II) ion and RY4 by BMDA are presented in Fig. 8. There was rapid uptake of the cadmium ions and reactive yellow 4 dye in the first 15 min for all the concentrations, followed by a gradual increase for the next 120 min after which there was no appreciable change in the amount adsorbed, inferring a dynamic equilibrium (120 to 240 min). The adsorption capacity at equilibrium increases from 23.1 to 134.3 mg/g and 22.1 to 88.1 mg/g for Cd(II) and RY4 respectively as the initial concentrations increases from 40 to 240 mg/L. The rapid uptake of the pollutant as observed at the early stage of the reaction is due to (i) availability of unoccupied active sites on the surface of the adsorbent and (ii) large driving force provided by the concentrations of the adsorbates at the initial stage of the adsorption process. However, as the reaction progresses, these active sites become saturated, thus leading to uniform adsorption at a contact time higher than 120 min. Similar reports had been documented in literature (Adeogun et al. 2013; Adeogun et al. 2013; Ofudje et al. 2017; Shappur et al. 2017). For this study, maximum uptake was attained at an agitation time of 120 min and initial adsorbate concentration of 240 mg/L.

Effect of pH on removal efficiency of the adsorbent

Chemistry of both the pollutants and adsorbent in aqueous solution depends on pH of the medium to a certain extent, invariably; therefore, solution pH is one of the significant factors upon which adsorption depends. The effects of pH on the uptake of Cd(II) ion and RY4 dye were examined by varying the solution pH between pH

Table 1 Lattice parameters and crystallite sizes of BMDA powders before and after adsorption

Samples	FWHM (°)	Parameter a (nm)	Parameter c (nm)	c/a	Parameter V (nm)	Crystallite size (nm)
BMDA	0.4345	0.9414	0.6873	0.72814	1.5770	57.32
BMDA + Cd	0.6691	0.9442	0.6855	0.7304	1.6859	73.41
BMDA + RY4	0.7354	0.9445	0.6868	0.73260	1.5862	81.73



of 3.5 to 9.5 and the results are as presented in Fig. 9. The uptake of Cd^{2+} increased drastically from 60.3 to 84.3% as the solution pH was raised from 3.5 to 6, while that of RY4 dye increases from 46.7 to 71.5% as pH increases from 3.5 to 4.5. At lower pH, contest arising from metal ions and hydrogen ions for the empty sites coupled with the positive density charge on the adsorbent sites which are both responsible for the lower removal efficiency as observed in the case of the metal ions. But as the solution pH increases, there is less competition by the hydrogen ions for the adsorption sites

due to deprotonation and this gives rise to better uptake of the metal ions (Adeogun et al. 2013; Adeogun et al. 2013; Ofudje et al. 2017; Shappur et al. 2017). However, the reduced uptake of Cd(II) observed at solution pH greater than 6 could be as a result of the formation of hydroxide or precipitation of oxide at higher solution pH (Adeogun et al. 2012; Han et al. 2012). On the contrary, since the RY 4 dye is anionic, lower solution pH in acidic medium favoured its adsorption owing to the positive electrostatic interaction between the BMDA and pollutants. On the other hand, the repulsive forces which

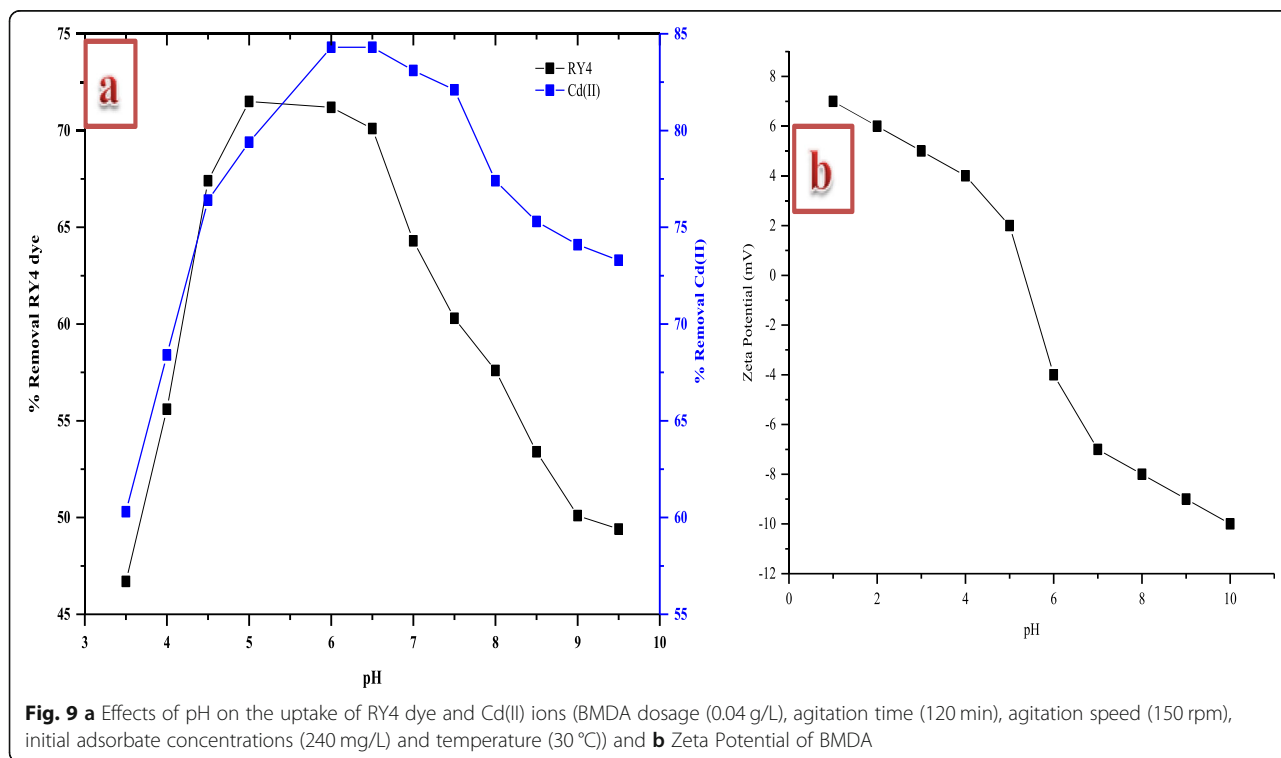
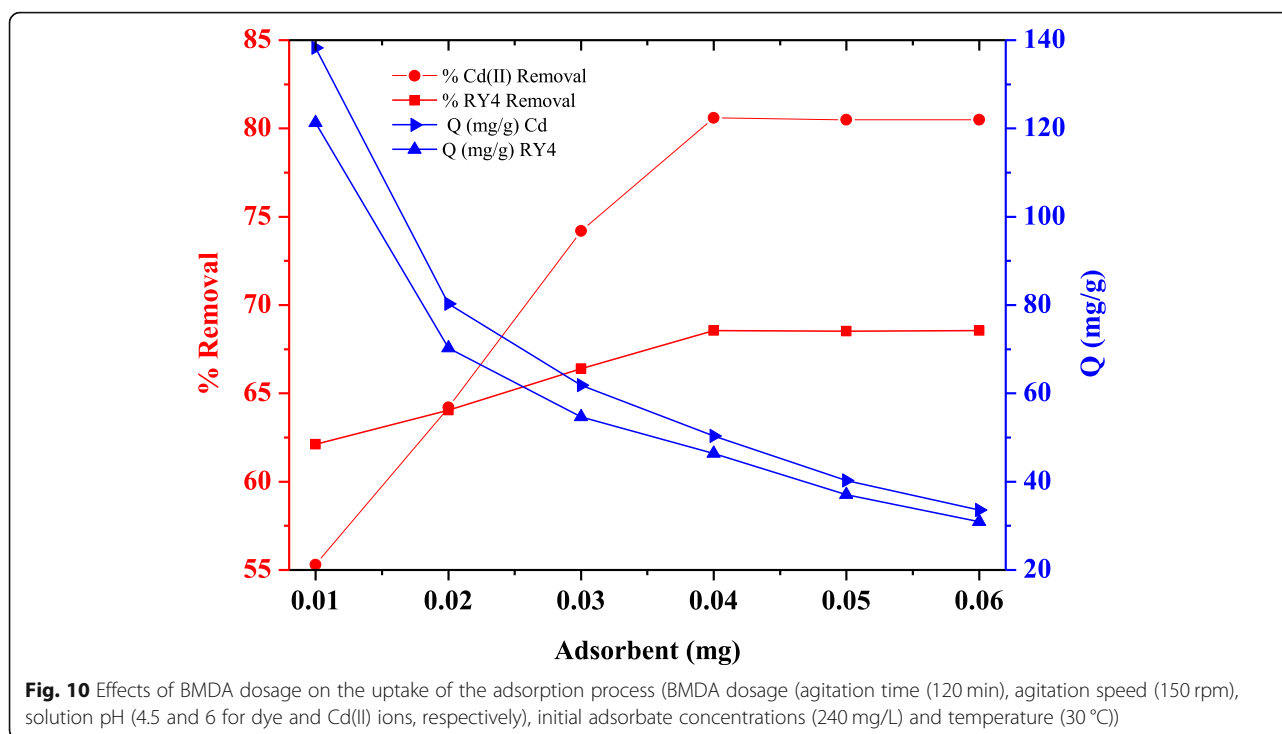


Fig. 9 a Effects of pH on the uptake of RY4 dye and Cd(II) ions (BMDA dosage (0.04 g/L), agitation time (120 min), agitation speed (150 rpm), initial adsorbate concentrations (240 mg/L) and temperature (30 °C)) and b Zeta Potential of BMDA



existed between the RY4 dye and the surface of the BMDA which is negatively charged could be the reason for the decline in the efficiency of the adsorption of the dye as observed at greater pH values (Adeogun and Babu, 2015; Shappur et al. 2017).

The impact of solution pH on the removal ability of the BMDA adsorbent can be further explained better using the principle of iso-electric point on the surface of the adsorbent. The functional groups on the surface of

the adsorbent at the pH of zero point of charge (pH_{zpc}) will have no contribution to the solution pH neither in acidic nor basic (Ofudje et al. 2017). For this present study, the zero point charge of BMDA (Fig. 9b) was obtained to be 5.3. At a solution pH less than the pH_{zpc}, the surface of the BMDA will be positively charged and is good for attracting anions (RY4 dye) from the solution. On the contrary, with a solution pH above the pH_{zpc} value, the surface of the BMDA is negatively

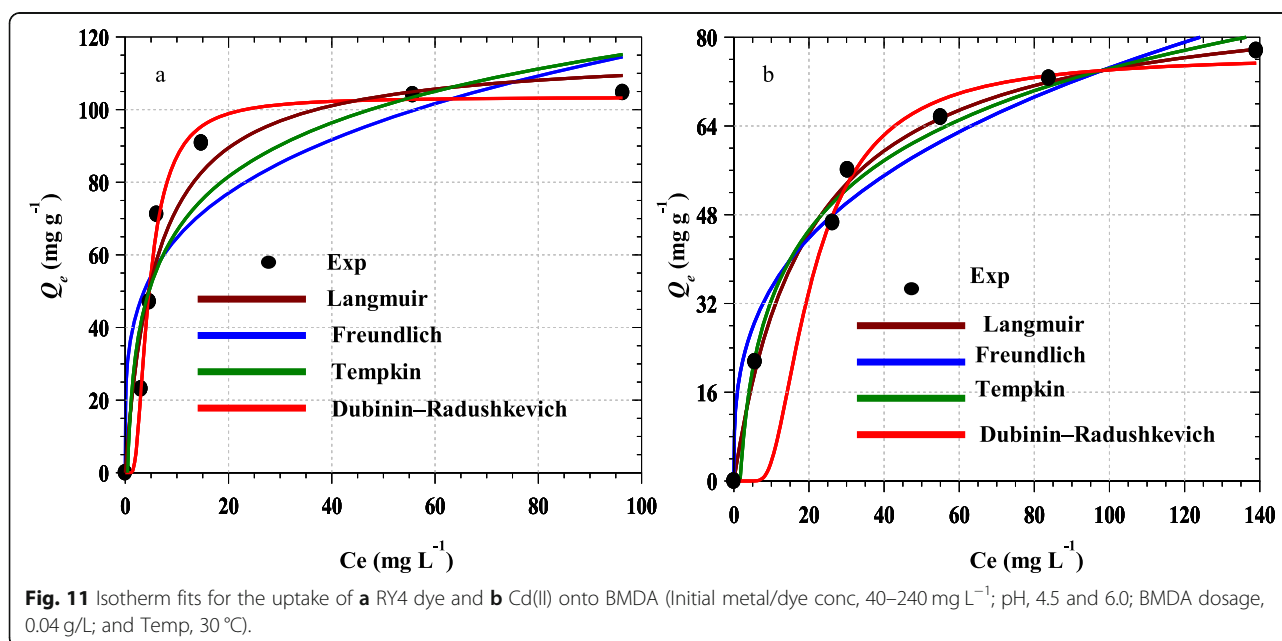


Table 2 Isotherm constants for the adsorption of Cd(II) ions and RY4 dye onto BMDA

Isotherms	Parameter	Cd(II)	RY4
Langmuir	Q_{\max} (mg g^{-1})	116.16	94.85
	b (L mg^{-1})	0.167	0.035
	R_L	0.056	0.209
	R^2	0.986	0.988
Freundlich	$K_F \times 10^2$ ($(\text{mol g}^{-1}) (\text{mol L}^{-1})^{-1/n}$)	36.15	16.32
	N	3.96	3.03
	R^2	0.964	0.985
Tempkin	a_T (L mg^{-1})	117.76	138.99
	b_T	2.25	0.604
	R^2	0.975	0.987
Dubin-Radushkevich	Q_s (mg g^{-1})	103.43	65.95
	$\beta \times 10^6$ (mol J^{-1}) ²	2.97	7.51
	E (kJ mol^{-1})	410.30	258.03
	R^2	0.998	0.971

charged and is good for attracting cations (Cd^{2+}). This further provides illumination on why the uptake of RY4 dye was favourable at a lower solution pH of 4.5 (less than 5.3 for pHzpc) and this increase in the uptake of

dye is due to the electrostatic force of attraction between the positively charged surface of the BMDA and the negatively charged dye ions, while an increase in the uptake of Cd^{2+} is enhanced at a solution pH of 6 (greater

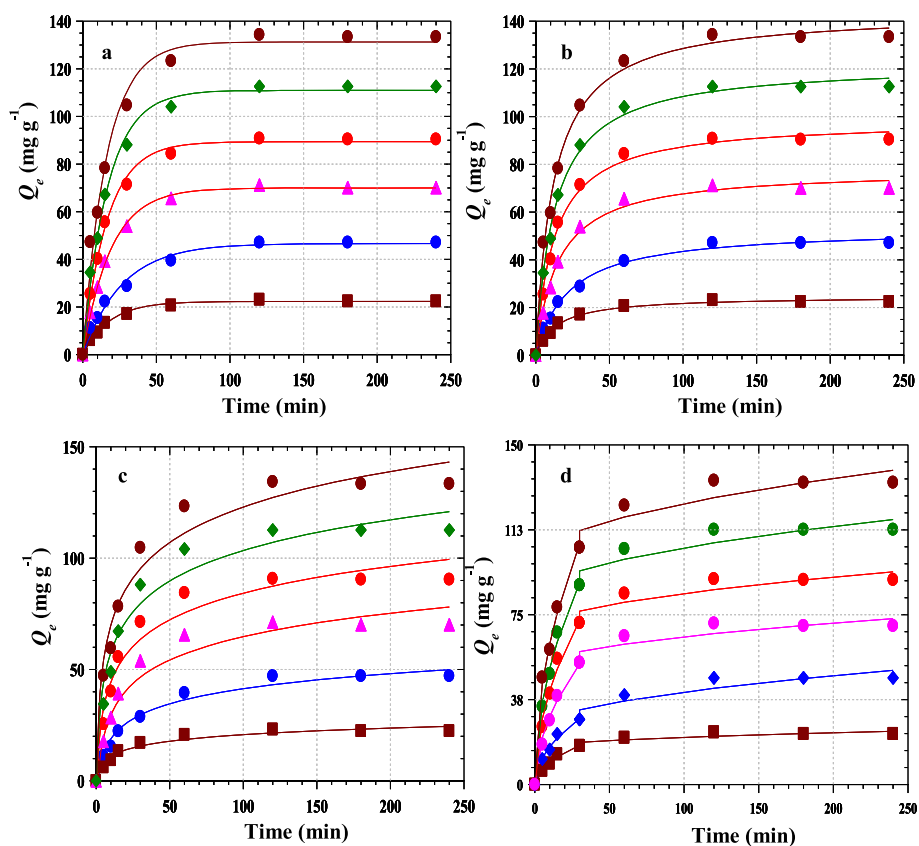


Fig. 12 Least square fit of Q_e versus t of kinetic plots for the removal of Cd(II) ions on BMDA **a** first-order, **b** second-order, **c** Elovich fits, and **d** intraparticle diffusion models (adsorbent dosage, 0.04 g/L; pH, 6.0; and temp, 30 °C)

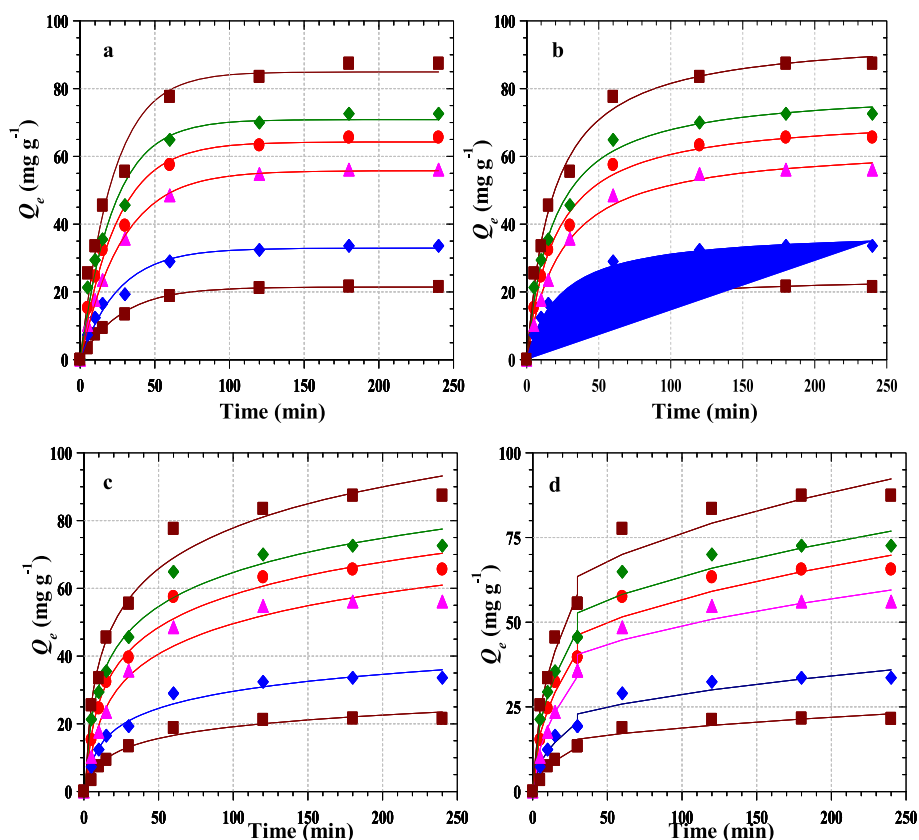


Fig. 13 Least square fit of Q_e versus t of kinetic plots for the uptake of Cd(II) ions on BMDA (a) first-order (b) second-order (c) Elovich fits and (d) Intraparticle diffusion models. (Adsorbent dosage: 0.04 g/L, Temp: 30 °C, pH: 4.5 for RY4 dye adsorption)

than 5.3 for pHzpc) is due to the electrostatic force of attraction between the negatively charged surface of the BMDA and the positively charged cadmium ions (Limei et al. 2015; Ofudje et al. 2017).

Effect of BMDA dosage on removal efficiency

The relationships between adsorbent dosage and the amount of pollutants adsorbed are presented in Fig. 10. The results indicated that the quantity adsorbed (milligrammes per gramme of adsorbent) decreases with increase in the dosage, which is as a result of aggregation leading to a decrease surface area. However, as BMDA dosage increases, the adsorption efficiency of Cd(II) ions and RY4 dye also increases. The maximum percentage removal was observed at BMDA dosage of 0.04 g and above this, no appreciable increase in the uptake of the pollutants was observed.

Adsorption isotherms

The four different isotherms used in the analysis of the adsorption behaviour of the pollutants unto the BMDA are as presented in Fig. 11 a and b. It is apparent from the parameters as deduced from the plots of the least square fits of the models that the

adsorption capacity (see Table 2) raises momentarily as a result of the accessibility of active unoccupied sites on the BMDA surface and this got saturated as the adsorbate concentrations increase. From the Langmuir isotherm, the maximum adsorption capacities (Q_{\max}) of 94.85 and 116.16 mg g^{-1} were achieved for the uptake of RY4 and Cd(II), respectively. The values of separation factor (R_L) and that of n from the Freundlich isotherm were observed to be above unity for all the adsorption and thus indicate favourable adsorption processes. The binding constants 138.99 and 117.76 mg L^{-1} obtained from Tempkin isotherm parameters for RY4 and Cd(II), respectively, showed that BMDA has the higher affinity for the dye than Cd(II) ions. The values of Q_s as obtained from D-R are 65.95 and 103.43 mg g^{-1} , respectively, for RY4 and Cd(II) ions adsorption. The values of E as obtained are 0.26 and 0.41 kJ mol^{-1} for RY4 and Cd(II) ions, respectively, thus suggesting physisorption as the adsorption process (Ofudje et al. 2017). Using the average values of correlation coefficient (R^2) as basis for comparison, the isotherm fit can be arranged as Langmuir > Dubinin-Radushkevich > Tempkin > Freundlich. This is in accordance with literature reported

Table 3 Kinetic parameters for the adsorption of Cd(II) ions and RY4 by BMDA

		Cd(II) ion					RY4 dye						
Pseudo-first order	C_o (mg/L)	40	80	120	160	200	240	40	80	120	160	200	240
	$Q_{e\text{ exp}}$ (mg g ⁻¹)	22.40	47.10	70.10	90.40	112.60	133.40	21.500	33.600	56.100	65.600	72.600	87.400
	$Q_{e\text{ cal}}$ (mg g ⁻¹)	22.31	46.63	69.97	89.38	110.95	131.27	21.439	32.924	55.763	64.256	70.858	84.916
	$k_1 \times 10^2$ (min ⁻¹)	0.055	0.037	0.052	0.060	0.060	0.062	0.036	0.039	0.036	0.041	0.045	0.046
	R^2	0.998	0.997	0.999	0.999	0.997	0.997	0.999	0.997	0.999	0.999	0.997	0.997
	%SSE	0.086	0.470	0.126	1.022	1.651	2.134	0.061	0.676	0.337	1.344	1.742	2.484
	RMSE	0.010	0.052	0.014	0.114	0.183	0.237	0.007	0.075	0.037	0.149	0.194	0.276
	HYBRID	0.055	0.144	0.026	0.163	0.213	0.232	0.041	0.293	0.086	0.299	0.351	0.418
Pseudo-second order	$Q_{e\text{ cal}}$ (mg g ⁻¹)	24.712	53.085	77.794	98.503	122.260	143.958	24.524	38.165	63.999	72.537	79.633	95.485
	$k_2 \times 10^4$ (g mg ⁻¹ min ⁻¹)	28.9	8.55	8.57	8.03	6.41	5.80	17.5	11.5	6.51	6.99	7.09	6.03
	R^2	0.992	0.994	0.992	0.994	0.996	0.996	0.998	0.998	0.999	0.998	0.998	0.998
	%SSE	2.312	5.985	7.694	8.103	9.660	10.558	3.024	4.565	7.899	6.937	7.033	8.085
	RMSE	0.257	0.665	0.855	0.900	1.073	1.173	0.336	0.507	0.878	0.771	0.781	0.898
	HYBRID	1.336	1.611	1.413	1.175	1.129	1.048	1.762	1.709	1.763	1.366	1.262	1.210
Elovich	$Q_{e\text{ cal}}$ (mg g ⁻¹)	21.59	43.45	67.75	87.40	107.64	127.63	20.033	30.918	51.958	60.684	67.390	81.052
	α (mg (g min) ⁻¹)	5.16	6.11	11.64	22.73	32.57	44.43	2.314	4.297	5.933	9.036	12.346	15.023
	β (g mg ⁻¹)	0.230	0.098	0.067	0.058	0.049	0.042	0.201	0.138	0.077	0.072	0.069	0.057
	R^2	0.992	0.996	0.991	0.992	0.993	0.994	0.995	0.996	0.995	0.996	0.996	0.996
	%SSE	0.813	3.648	2.348	2.996	4.964	5.768	1.467	2.682	4.142	4.916	5.210	6.348
	RMSE	0.090	0.405	0.261	0.333	0.552	0.641	0.163	0.298	0.460	0.546	0.579	0.705
Intraparticle diffusion	K_{1d} (mg g ⁻¹ min ^{-0.5})	3.23	5.37	10.05	13.47	16.40	19.15	2.53	3.72	6.57	7.54	8.43	10.38
	C_1 (mg g ⁻¹)	-0.34	-0.31	-1.81	-1.18	-0.63	1.50	-0.72	0.11	-1.98	0.15	1.49	1.39
	R^2	0.996	0.997	0.997	0.996	0.998	0.998	0.991	0.992	0.994	0.995	0.998	0.996
	K_{2d} (mg g ⁻¹ min ^{-0.5})	0.49	1.75	1.45	1.73	2.26	2.66	0.75	1.30	1.90	2.35	2.41	2.87
	C_2 (mg g ⁻¹)	15.96	23.38	50.73	67.08	81.95	97.54	11.37	15.78	30.05	33.35	39.55	47.76
	R^2	0.997	0.994	0.997	0.998	0.998	0.998	0.994	0.992	0.995	0.993	0.994	0.995

that experimental data for the adsorption processes exhibited best fitting with the Langmuir isotherm model (Shappur et al. 2017).

Mechanism and kinetics of adsorption

The kinetics of Cd(II) ions and RY4 dye adsorption on BMDA were studied to understand optimum operational conditions, which are a significant criterion in describing the mechanism and the adsorption efficiency. Figures 12 and 13 give the plots of pseudo-first-order, pseudo-second-order, and Elovich and intraparticle diffusion models for the analysis of the time-dependent adsorption of Cd(II) ions and RY4 dye, respectively, by BMDA while the parameters for these fits are presented in Table 3. From the analysis of the kinetic data as presented in Table 3, although the values of correlation coefficient R^2 for both pseudo-first-order and pseudo-second-order kinetic models are close to unity, the pseudo-first-order

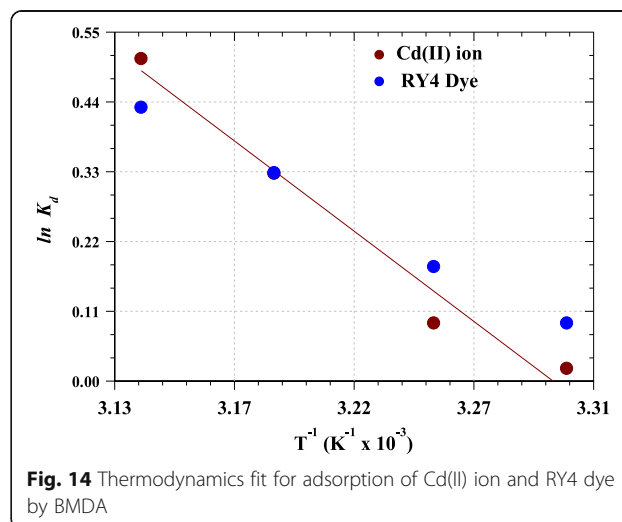


Fig. 14 Thermodynamics fit for adsorption of Cd(II) ion and RY4 dye by BMDA

Table 4 Thermodynamic values for uptake of RY4 dye and Cd(II) ion by BMDA

Temp (K)	Cd(II) ions					RY4 dye				
	K_d	ΔG (J mol ⁻¹)	ΔH (kJ mol ⁻¹)	ΔS (J mol ⁻¹ K ⁻¹)	R^2	K_d	ΔG (J mol ⁻¹)	ΔH (kJ mol ⁻¹)	ΔS (J mol ⁻¹ K ⁻¹)	R^2
303	1.02	-49.24	26.28	86.57	0.989	1.11	-251.76	18.02	60.16	0.999
308	1.11	-255.92				1.20	-461.75			
313	1.39	-850.95				1.39	-853.99			
318	1.66	-1342.47				1.54	-1140.71			

model was deemed as the best fit due to the consistency observed in the values of the calculated adsorption capacity ($Q_{e\text{ calc}}$) with that of the experimental values ($Q_{e\text{ exp}}$). Furthermore, it was noted that the error margins from the first-order model are lower than those obtained for second-order. Careful analysis of the Elovich model's parameters as listed in Table 3 indicated a rise in rate of adsorption just as the pollutants concentration increases as inferred by α and the reduction in rate of desorption (β) with increased pollutants concentrations which suggest the existence of chemical bond interactions between the various functional groups present on the BMDA and pollutants (Shappur et al. 2017).

The intraparticle diffusion model was investigated in order to further understand the mechanisms of the adsorption processes. Two diffusion stages were observed for the process; the first stage is rapid and occurs in the first 30 min of the adsorption, while the second which is a relaxed stage proceeds till equilibrium. The increase intraparticle diffusion rate constant (K_{id}) with contaminant concentration may be as a result of the opposition of the surface boundary of BMDA to the rise in the driving force with the gradient concentration as these solutes access the available sites on the adsorbent (Shappur et al. 2017). When compared, the values of K_{id} suggested that Cd(II) ions diffused faster than the RY4 dye molecule at an initial stage, while the reverse was observed at the second stage. It was also observed that the beginning of the adsorption process was made up of intraparticle diffusion as evident from the values of the intercepts C_i obtained and more significantly by the external mass transfer (Adeogun and Babu, 2015).

Thermodynamic study

van't Hoff plot $\ln K$ against the inverse of temperature for Cd(II) ion and RY4 dye adsorptions are shown in Fig. 14 with the thermodynamic parameters as listed Table 4.

It was observed that the values of ΔG° were negative which is an indication of the spontaneous process and as such, thermodynamically favoured. The increase in the negative values of standard energy change (ΔG°) with temperature is an indication that

the process is favoured. Since values of standard enthalpy change (ΔH°) obtained were positive, it is an indication that the process is endothermic. Similarly, the positive values of standard entropy change (ΔS°) obtained imply an increase in the randomness of the adsorption process (Adeogun and Babu, 2015; Shappur et al. 2017).

Conclusion

This study shows the possibility of obtaining apatite material from bone meal and its subsequent use for adsorption removal of RY 4 dye and Cd(II) ion simultaneously via batch process. The adsorption process depended on agitation time, solution pH, initial RY 4 dye and Cd(II) concentration, BMDA dosage and temperature of the reaction medium. The isotherm studies suggest that all the tested isotherms fit well with data of the Langmuir isotherm as the maximum monolayer adsorption capacities of for RY4 dye and Cd(II) ions were obtained to be 94.85 and 116.16 mg/g, respectively. Kinetic analysis revealed that the pseudo-first-order model was most suitable to explain the behaviour of the adsorption process thus suggesting the adsorption mechanism to be physisorption. The thermodynamic parameters of enthalpy change, free energy change and entropy changes proved that the adsorption of RY4 dye and Cd(II) ions is endothermic, spontaneous, feasible which is also random in nature. It is therefore apparent that the applicability of bone-derived hydroxyapatite adsorbent for the adsorption of pollutants as discussed here is helpful in adsorption engineering application.

Abbreviations

a_T : Tempkin constants relating to binding constant (Lmg⁻¹); b : Langmuir equilibrium constant (L mg⁻¹); BMDA: Bone meal-derived apatite; b_T : Heat of adsorption; C_e : Equilibrium concentrations; C_0 : Initial concentrations; D-R: Dubinin-Radushkevich; E : Mean free energy (kJ mol⁻¹); EDX: Energy-dispersive X-ray analysis; FT-IR: Fourier-transform infrared spectroscopy; HYBRID: Composite fractional error; k_1 : Adsorption rate constant (min⁻¹) for a first-order; k_2 : Rate constant of pseudo-second-order (g mg⁻¹ min⁻¹); K_d : Equilibrium constant; K_F : Adsorption capacity; m : Adsorbent mass (g); n : Adsorbent intensity; pH_{zpc}: The pH of zero point of charge; Q_e : Amount of adsorbate adsorbed in mg/g; Q_{max} : Maximum amount of solute adsorbed; Q_s : Represents the saturation capacity (mol g⁻¹); R : Molar gas constant (8.314 J mol⁻¹ K⁻¹); R^2 : Correlation coefficient; R_L : Separation factor; RMSE: Root mean square error; RY4 dye: Reactive yellow 4 dye; SEM: Scanning electron microscope; SSE: Sum of square error function; T : Temperature (K); TEM: Transmission electron microscope; TGA: Thermogravimetric analysis; V : Volume (L) of the pollutant taken; XRD: X-ray diffractometer; β : Mean free

energy of adsorption; ΔG° : Free energy change; ΔS° : Entropy change; ΔH° : Enthalpy change; ϵ : Polanyi potential

Acknowledgements

All authors are grateful to NAM S&T Centre Research Training Fellowship for Developing Country Scientists (RTF-DCS), Government of India, for the financial support given to Dr. Ofudje to carry out this work. Thanks are also extended to all the technical staff of CSIR-CECRI, India, for their supports during characterization.

Authors' contributions

All authors have equal contribution to this research work. All authors read and approved the final manuscript.

Funding

This project is supported by NAM S&T Centre Research Training Fellowship for Developing Country Scientists (RTF-DCS), Government of India.

Availability of data and materials

Data sharing not applicable to this article

Competing interests

The authors declare that they have no competing interests.

Author details

¹Department of Chemical Sciences, Mountain Top University, Prayer City, Ibafo, Nigeria. ²Department of Chemistry, Federal University of Agriculture, Abeokuta, Nigeria. ³Department of Microbiology, Federal University of Agriculture, Abeokuta, Nigeria.

Received: 23 May 2019 Accepted: 5 February 2020

Published online: 13 February 2020

References

- Adeogun AI, Babu RB. One-step synthesized calcium phosphate-based material for the removal of alizarin S dye from aqueous solutions: isothermal, kinetics, and thermodynamic studies. *Appl Nanosci*. 2015;1–3.
- Adeogun AI, Idowu MA, Ofudje AE, Kareem SO, Ahmed SA. Comparative biosorption of Mn(II) and Pb(II) ions on raw and oxalic acid modified maize husk: kinetic, thermodynamic and isothermal studies. *Appl Water Sci*. 2013;3:167–79.
- Adeogun AI, Ofudje AE, Idowu MA, Ahmed SA. Kinetic, thermodynamic and isothermal parameters of biosorption of Cr(VI) and Pb(II) ions from aqueous solution by biosorbent prepared from corncob biomass. *Inorg Chem Ind J*. 2012;7:119–29.
- Adeogun AI, Ofudje EA, Idowu MA, Kareem SO, Vahidhabanu S, Ramesh RB. Biomass derived hydroxyapatite for the effective removal of reactive yellow 4 dye: equilibrium, kinetic and thermodynamic studies. *ACS, Omega*. 2018;3:1991–2000.
- Allen SJ, McKay G, Porter JF. Adsorption isotherm models for basic dye adsorption by peat in single and binary component systems. *J Colloid Interf Sci*. 2004;280:322–33.
- Barakat MA. New trends in removing heavy metals from industrial wastewater. *Arab J Chem*. 2011;3:1:3 doi 61–77. <https://doi.org/10.1016/j.arabjc.2010.07.019>.
- Chen X, Wright JV, Conca JL, Peurrung LM. Evaluation of heavy metal remediation using mineral apatite. *Wat Air Soil Poll*. 1997;98:57–8.
- Cheng XM, Niu YMD, Ding QB, Yin XM, Huang GB, Peng JMD, Song JM. Cadmium exposure and risk of any fracture: a PRISMA-compliant systematic review and meta-analysis. *Medici*. 2016;95:1–7.
- Feng Y, Gong JL, Zeng GM, Niu QY, Zhang HY, Niu CG, Deng JH, Yan M. Adsorption of Cd(II) and Zn(II) from aqueous solutions using magnetic hydroxyapatite nanoparticles as adsorbents. *Chem Engine J*. 2010;162:487–94.
- Fumiaki M, Yoshiteru K, Yoko S. Formation and structure of zinc-substituted calcium hydroxyapatite. *Mater Res Bull*. 2005;40:209–20.
- Han KL, Tjoon TT, Mahamad HI, Anees A, Hui TC. Adsorption and removal of zinc(II) from aqueous solution using powdered fish bones. *APCBEE Procedia*. 2012;1:96–102.
- Janegitz BC, Figueiredo-Filho LCS, Marcolino-Junior LH, Souza SPN, Pereira-Filho ER, Fatibello-Filho O. Development of a carbon nanotubes paste electrode modified with crosslinked chitosan for cadmium(II) and mercury(II) determination. *J Electroanal Chem*. 2011;660:209–16.
- Langmuir I. The adsorption of gases on plane surfaces of glass, mica, and platinum. *J Am Chem Soc*. 1918;40:1361–403.
- Limei C, Yaoguang W, Lihua H, Liang G, Bin D, Qin W. Mechanism of Pb(II) and methylene blue adsorption onto magnetic carbonate hydroxyapatite/graphene oxide. *RSC Adv*. 2015;5:9759–70.
- Lin GH, Brusick DJ. Mutagenicity studies on two triphenylmethane dyes, bromophenol blue and tetrabromophenol blue. *J Appl Toxicol*. 1992;12:267–74.
- Nasser AM, Myung SK, Omran AM, Faheem AS, Hak YK. Extraction of pure natural hydroxyapatite from the bovine bones bio waste by three different methods. *J Mat Proc Tech*. 2009;209:3408–15.
- Ngah WW, Teong LC, Hanafiah MA. Adsorption of dyes and heavy metal ions by chitosan composites: a review. *Carbohydr Polym*. 2011;83:1446–56.
- Nzihou A, Sharrock P. Role of phosphate in the remediation and reuse of heavy metal polluted wastes and sites. *Waste Biomass Valor*. 2010;1:163–74.
- Ofudje EA, Awotula AO, Hambate GV, Akinwunmi F, Alayande SO, Olukanni OD. Acid activation of groundnut husk for copper adsorption: kinetics and equilibrium studies. *Desal Water Treat*. 2017;86:240–51.
- Rengaraj S, Kim Y, Joo CK, Yi J. Removal of copper from aqueous solution by aminated and protonated mesoporous aluminas: kinetic and equilibrium. *J Colloid Interf Sci*. 2004;273:14–21.
- Schmuhl R, Krieg HM, Keizer K. Adsorption of Cu(II) and Cr(VI) ions by chitosan: kinetics and equilibrium studies. *Water Sal*. 2001;27:1–8.
- Shappur V, Karuprasamy D, Adeogun AI, Ramesh B. Impregnation of zinc oxide modified clay over alginate beads: a novel material for the effective removal of Congo red from wastewater. *RSC Adv*. 2017;7:5669.
- Shawabkeh RA, Tutunji MF. Experimental study and modeling of basic dye sorption by diatomaceous clay. *Appl Clay Sci*. 2004;24:111–20.
- Shukla SR, Pai RS. Adsorption of Cu (II), Ni (II) and Zn (II) on dye loaded groundnut shells and sawdust. *Separ Purify Tech*. 2005;43:1–8.
- Smiciklas I, Dimovic S, Plecas I, Mitric M. Removal of Co²⁺ from aqueous solutions by hydroxyapatite. *Water Resear*. 2006;40:2267–74.
- Sun Q, Yang L. The adsorption of basic dyes from aqueous solution on modified peat-resin particle. *Water Resear*. 2003;37:1535–44.
- Wang S, Soudi M, Li L, Zhu ZH. Coal ash conversion into effective adsorbents for removal of heavy metals and dyes from wastewater. *J Hazard Mat*. 2005;133:243–51.
- Xiaoqin L, Yunwen L, Hejun G. Enhancement adsorption of hexavalent chromium from aqueous solution on polypyrrole using ethylamine group. *J Disper Sci Technol*. 2017. <https://doi.org/10.1080/01932691.2017.1404917>.
- Yang X, Chen C, Li J, Zhao G, Ren X, Wang X. Graphene oxide-iron oxide and reduced graphene oxide-iron oxide hybrid materials for the removal of organic and inorganic pollutants. *RSC Adv*. 2012;2:8821–6.
- Zhao G, Li J, Ren X, Chen C, Wang X. Few-layered graphene oxide nanosheets as superior sorbents for heavy metal ion pollution management. *Environ Sci Technol*. 2011;45:10454–62.

Publisher's Note

Springer Nature remains neutral with regard to jurisdictional claims in published maps and institutional affiliations.

Submit your manuscript to a SpringerOpen® journal and benefit from:

- Convenient online submission
- Rigorous peer review
- Open access: articles freely available online
- High visibility within the field
- Retaining the copyright to your article

Submit your next manuscript at ► [springeropen.com](https://www.springeropen.com)